Carbon 142 (2019) 504–512

Contents lists available at ScienceDirect

Carbon

journal homepage: www.elsevier.com/locate/carbon

MoS_2-graphene heterostructures as efficient organic compounds sensing 2D materials

Tung Pham [a], Pankaj Ramnani [a], Claudia C. Villarreal [b], Jhoann Lopez [a], Protik Das [c], Ilkeun Lee [d], Mahesh R. Neupane [e, **], Youngwoo Rheem [b], Ashok Mulchandani [a, b, *]

[a] Department of Chemical and Environmental Engineering, University of California–Riverside, Riverside, CA, 92521, United States
[b] Materials Science and Engineering Program, University of California–Riverside, Riverside, CA, 92521, United States
[c] Department of Electrical and Computer Engineering, University of California–Riverside, Riverside, CA, 92521, United States
[d] Department of Chemistry, University of California–Riverside, Riverside, CA, 92521, United States
[e] U. S. Army Research Laboratory, 2800 Powder Mill Rd, Adelphi, MD, 20783, USA

ARTICLE INFO

Article history:
Received 5 September 2018
Received in revised form
23 October 2018
Accepted 24 October 2018
Available online 26 October 2018

ABSTRACT

In this work, electrical properties and application for volatile organic compounds detection of molybdenum disulfide (MoS_2)–graphene (MS/G) heterostructure is investigated. The MS/G heterostructure is synthesized by physical stacking of single-layer (SL) MoS_2 over SL graphene. The difference in the work-functions between the MoS_2 and graphene leads to electron transfer from MoS_2 to graphene, which changes FET charge neutrality point (V_{CNP}) of graphene by as much as 30 V and increases the electron-to-hole ratio in graphene. This charge transport phenomenon is further confirmed by shifting of Raman G peak and quenching of photoluminescence intensity by 50% of MoS_2 in the heterostructure. Ultraviolet photoelectron spectroscopy reveals a 0.1 eV upshift of the Fermi level of graphene in MS/G, which is consistent with the electrical double-layer capacitance versus the electrode potential measurement and energy band alignment predicted by first-principle simulations. The heterogenity induced charge transfer in the heterostructure of MS/G results in outstanding performance in chemical sensing. The MS/G FET shows improved stability in dry air with negligible shifting of V_{CNP}, as compared to graphene FET. In the detection of toluene, the MS/G FET-based sensor shows higher sensitivity and superior signal-to-noise ratio compared to MoS_2 or graphene individually.

Published by Elsevier Ltd.

1. Introduction

Two-dimensional (2D) van der Waals (vdW) materials including graphene and transition metal dichalcogenides (TMDs) have recently gathered increasing interests in research communities owing to their intriguing electrical, thermal and optical properties [1]. Graphene consists of sp^2-bonded carbon atoms arranged in a honeycomb lattice and exhibits exceptional properties such as high carrier mobility up to 10^5 $cm^2V^{-1}s^{-1}$ at room temperature, thermal conductivity above 3000 $Wm^{-1}K^{-1}$, and high optical transparency (~97.7%) [2]. However, the absence of a band gap in graphene has limited its applications in electronic devices.

TMDs, chemically abbreviated as MX_2, where M is a transition metal atom (Mo, W, etc.) and X is a chalcogen atom (S, Se, Te, etc.), exhibit a wide range of electrical properties from insulating or semi-conducting to metallic depending upon their crystalline phase [3,4]. One of the most widely researched TMD is molybdenum disulfide (MoS_2). This semi-conducting material possesses an indirect band gap of 1.29 eV in its bulk form but transitions to a direct band gap of 1.9 eV in single layer (SL) structure [5,6]. Due to this sizable band gap, FETs using MoS_2 as the conducting channel exhibit high on/off ratios in the range of 10^4-10^6 and very low power leakage in off-state [7]. However, usage of MoS_2 as a channel material for the future devices is limited by its low charge mobility in the range of ~0.1–100 $cm^2V^{-1}s^{-1}$ [8]. Additionally, due to the presence of a high Schottky barrier between metal contacts and MoS_2 layers and poor interface quality, the transport in channel is susceptible to high contact resistance [9].

One of the proposed solutions to mitigate these limitations is

* Corresponding author. Department of Chemical and Environmental Engineering, University of California–Riverside, Riverside, CA, 92521, United States.
** Corresponding author. U. S. Army Research Laboratory, 2800 Powder Mill Rd, Adelphi, MD, 20783, USA.
E-mail addresses: mahesh.r.neupane.civ@mail.mil (M.R. Neupane), adani@engr.ucr.edu (A. Mulchandani).

https://doi.org/10.1016/j.carbon.2018.10.079
0008-6223/Published by Elsevier Ltd.

fabrication of a heterostructure that can utilize the complementary properties of MoS_2 and graphene, such as high carrier mobility and Schottky barrier tunability of graphene and sizable band gap of MoS_2 [10]. Similar to the constituent layered materials, these heterostructures are held together by weak interlayer vdW forces. Prior studies on graphene-TMD heterostructures have relied on artificial stacking of individual 2D crystals using mechanical exfoliation and stamping, which usually results in atomically sharp interfaces that are free from any polymer/chemical residue [11,12]. However, mechanical exfoliation of 2D crystals is not a scalable approach, and hence, not suitable for commercial applications. A more scalable approach of fabricating such 2D heterostructures is via physical stacking of thin films synthesized via CVD [13–18].

FET-based sensors are of interest since they allow on-chip integration of thin films including graphene and TMDs for label-free, highly sensitive and rapid detection of chemicals/biomolecules by fabricating low-power, inexpensive, portable devices. In these thin film FET-based sensors, any surface perturbation created by affinity-based binding or adsorption of chemicals leads to change in the current between the source and drain electrodes due to the extremely high surface area-to-volume ratio of the channel material, and this allows for label-free sensing applications. There have been multiple reports in literature on FET-based sensors that utilize graphene or MoS_2 as the channel material [19–21]. Though these ultra-scaled homogeneous 2D FETs exhibit promise as sensors and flexible electronics, the operational parameters are far from the desired values mainly due to poor surface quality leading to inefficient selectivity and low signal-to-noise ratio (SNR).

In this paper, we investigate the performance of MoS_2/graphene, hereafter referred to as MS/G, based FETs for chemical sensing of volatile organic compounds (VOCs) such as toluene. High quality graphene and MoS_2 thin film were synthesized using CVD on polycrystalline copper and sapphire substrate, respectively, and physically stacked on a Si/SiO_2 substrate to obtain MS/G. FET devices were fabricated with graphene, MoS_2 or MS/G as the channel material and 300 nm Si as the back gate. Upon stacking of MoS_2 over graphene, we observed significant photoluminescence (PL) quenching of MoS_2 and a shift in charge neutrality point (V_{CNP}) to lower gate voltage in MS/G FET as compared to graphene FET due to n-doping effect in graphene. The shift in energy level for the heterostructure is further explained and confirmed by ultraviolet photoelectron spectroscopy (UPS), electrical double layer-capacitance (C_{EDL}) versus voltage and first-principle simulations. These observations were in-line with the results obtained for other graphene-TMDC heterostructures fabricated by mechanically exfoliated crystals and paves the way for exploring CVD as a scalable route for fabrication of high quality vdW heterostructures [22–24]. We also observed that unlike the graphene FET, the MS/G FET was less susceptible to doping from ambient air and showed excellent stability with negligible shift of V_{CNP} in dry air over time. This stability and robustness of the channel material is vital for FET-based sensors that rely on shift in transfer characteristics for sensitive detection of chemicals with low limit of detection. Finally, we compared the performance of graphene, MoS_2 and MS/G FETs for dynamic sensing of toluene vapor by performing chronocurrent measurements. The response of the three FETs to toluene has shown MS/G based device has the highest sensitivity and selectivity due to its high surface area-to-volume ratio and high SNR ratio.

2. Experimental section

2.1. Synthesis of graphene and MoS_2

2.1.1. Graphene

SL graphene was synthesized using the method recently reported by our group to produce single, uniform crystals of graphene with diameter larger than 300 μm [25]. A 2×2 cm^2 piece of polycrystalline copper foil is inserted into a 1 in. quartz tube furnace and heated to 1030 °C in the presence of H_2 (10 sccm) and argon (300 sccm) gases and held at these conditions for 2 h. For graphene growth, diluted CH_4 in argon (90 ppm) is introduced for 20 min while H_2 flow remains unchanged. The foil is then cooled to room temperature under H_2 and argon gas flow. The graphene/copper foil is coated with PMMA and copper is then etched in 0.2 M ammonium persulfate (APS) solution. The floating graphene/PMMA is washed multiple times with deionized (DI) water in order to remove remaining residues. This PMMA/graphene stack is transferred onto a Si/SiO_2 wafer that is pre-cleaned in piranha solution (3:1 vol ratio of H_2SO_4:H_2O_2) and the PMMA layer is removed in acetone at 60 °C overnight.

2.1.2. MoS_2

A CVD method is employed with sulfur and molybdenum trioxide (MoO_3) as the growth precursors and sapphire as the substrate. The growth is carried out in the presence of argon flow at 50 sccm under ambient pressure. The substrate is placed facing down on top of the MoO_3 source at the center of the furnace, where the temperature is ramped from room temperature to 650 °C at a ramp rate of 25 °C min^{-1}. Sulfur is introduced to the system by evaporation using a heating jacket at 170 °C as soon as the furnace is turned on. When the furnace reaches 650 °C, the temperature is held constant for 10 min. Then, both the furnace and heating jacket are turned off and cooled down to room temperature. For the transfer, MoS_2 on sapphire is spin-coated with polystyrene (PS) and the PS/MoS_2 stack is isolated using simple lift-off in DI water, which does not require any etching process. The PS/MoS_2 film is washed several times with DI water to remove remaining residues and PS is removed by immersing in toluene solution.

2.2. Fabrication of FET devices

2.2.1. Graphene FET device

PMMA/graphene film is transferred onto pre-patterned gold electrodes and PMMA is removed in acetone at 60 °C. The collected large-area graphene film is patterned in a 50 μm × 10 μm pattern using conventional photolithography and the excess graphene is removed by reactive ion etching process with O_2 plasma. Photoresist on patterned graphene is cleaned overnight in acetone at 60 °C. Finally, 10 nm/100 nm in thickness of Cr/Au, respectively, is deposited on the back Si interface acting as a back-gate electrode.

2.2.2. MS/G FET device

After graphene FET is fabricated, PS/MoS_2 film is transferred onto the patterned graphene and air-dried for 1 h. The polystyrene layer is removed in toluene and the resulting device is annealed in 300 sccm Ar at 200 °C to remove remaining residues and also enhance the contact between graphene and MoS_2 layers. Finally, 10 nm/100 nm in thickness of Cr/Au, respectively, is deposited on the back Si interface acting as a back-gate electrode.

2.3. Electrochemical characterization

4-layer graphene is prepared by repeated stacking of PMMA-coated graphene onto SL graphene/copper. This method avoids PMMA contamination in the interlayer of multi-layer graphene, as only the top layer is coated with PMMA. For the MoS_2/4LG device, a layer of PS/MoS_2 is stacked onto the fourth graphene/copper layer and the PS is dissolved in toluene. Then, the PMMA/3LG is scooped on top. The pristine and doped PMMA/4LG are transferred onto glass. The PMMA layer is dissolved using acetone and a Cr/Au

contact (10 nm/140 nm) is evaporated surrounding a circular graphene area of 0.13 cm^2. The Cr/Au contact is insulated with PMMA for the electrochemical measurement, to leave only graphene exposed to the electrolyte. The electrochemical measurements is performed with a CHI 660C electrochemical station. The impedance of the electrodes is measured at a relatively high concentration of 0.5 M KCl, to make diffusion capacitance negligible with respect to the total C_{EDL}. An AC voltage with a frequency of 10 kHz and a perturbation amplitude of 5 mV is swept from −0.8 to 0.6 V using a Ag/AgCl reference electrode (saturated KCl) and a Pt mesh counterelectrode. The impedance of the MoS_2/4LG device is measured before and after annealing at 200 °C in Ar atmosphere.

2.4. Theoretical Modeling

Our calculations are based on first-principles density functional theory (DFT) using the projector augmented wave method and the Perdew-Burke-Ernzerhof (PBE) type generalized gradient approximation as implemented in the software package VASP [26–28]. More details are discussed in the Supplemental Information (SI). In brief, spin-orbit coupling (SOC) is included during self-consistent charge calculations. To improve the accuracy of the work-function calculations calculated from the PBE functional, we also carry out calculations using the Heyd-Scuseria-Ernzerhof (HSE) hybrid functional [29]. The HSE calculations incorporate 25% short-range Hartree-Fock exchange and the screening parameter is set to 0.2 Å. A Monkhorst-Pack scheme is adopted to integrate over the Brillouin zone with a converged k-mesh of $2 \times 8 \times 1$ for the surface and the heterostructure. A plane-wave basis cutoff of 550 eV is used. The atomic coordinates are optimized using the DFT-D2 dispersion correction [30]. All the relaxations are applied until all the interatomic forces are below 0.01 $eVÅ^{-1}$. For the calculations of the few-layer and monolayer structures with a vacuum distance of 20 Å is used to avoid interactions between the periodically repeated slabs. The MoS_2/graphene heterostructure is created using Cell-match Method [31]. To handle the in-plane lattice mismatch of ~9% between graphene and MoS_2 unit cells, the graphene unit cell is repeated 5 times, while the MoS_2 unit cell is repeated 3 times. The layer-to-layer strain is further reduced to ~5% by rotating graphene supercell by -R30° while fixing the MoS_2 super cell.

2.5. Optical, spectrometric and electrical characterization

Optical images are taken by Hirox KH-7700 digital microscope and AFM images are taken by Assylum Research MFP-3D Atomic Force Microscope. Both Raman spectra and PL measurements are collected by Horiba LabRam using a green laser ($\lambda = 532$ nm) for excitation. A minimal power of 5 mW is used to avoid local heating and possible damage to the materials. Characteristics curves of the FET devices are obtained by Keithley 2636 system by applying a constant $V_{source\text{-}drain} = 0.1$ V while sweeping the back gate voltage from −20 V to 120 V.

2.6. Gas sensing set-up and measurement

For stability of the devices in dry air and NO_2 detection, the flow rates of dry air and NO_2 are controlled by two mass flow controllers. The target concentration of NO_2 gas for detection is varied by changing the ratio of NO_2 and dry air's flow rates. The two gas streams are well-mixed in a mixer prior to being fed into the gas chamber.

For toluene detection, the set-up consists of an incoming carrier gas (dry air) which branches into two air streams. One stream is directed through a bubbler containing pure toluene solution in order to create a saturated toluene gas flow. This saturated toluene gas flow is then diluted and well-mixed with the other dry air gas stream in a mixer tube to desired concentrations. This resulting gas stream is fed into the gas chamber capped on the sensor for real-time detection.

For all gas detection measurements, a constant bias $V_{source\text{-}drain} = 0.1$ V is applied. Both current and resistance are monitored by the aforementioned Keithley system.

3. Result and discussion

Both SL graphene and SL MoS_2 were synthesized using CVD method, which is discussed in the experimental section, and then characterized using optical and electron microscopy, Raman spectrometry, atomic force microscope (AFM) and PL. Graphene was initially grown on polycrystalline copper substrate, according to our previous report, in a hexagonal crystal structure as shown in Fig. 1(a) and then transferred onto SiO_2 via a metal etching process with the aid of flexible polymer layer [25]. The uniform color contrast in Fig. 1(b) indicates that the graphene is single layer and residue-free after the transfer process. In addition, the absence of the D peak at 1260 cm^{-1} in the Raman spectra of our CVD graphene denotes there are no defects introduced during both the growth and transfer processes [32]. The ratio of the G peak at 1570 cm^{-1} and 2D peak at 2650 cm^{-1}, $I_{2D}/I_G \approx 2$, confirms our CVD graphene is single layer and uniform across the film [33].

On the other hand, MoS_2 was synthesized via CVD on two different substrates: sapphire and SiO_2. We observe that MoS_2 grows in a more continuous and uniform film on sapphire substrate than on SiO_2 substrate as seen in Fig. 2(a) and (b), respectively. For the device fabrication, we have used CVD-grown MoS_2 on sapphire which grows in more continuous film and comprises of mainly SL-MoS_2. The thickness of the MoS_2 film, which was initially synthesized on sapphire substrate and later transferred to SiO_2/Si substrate for device fabrication, is measured using AFM. The height

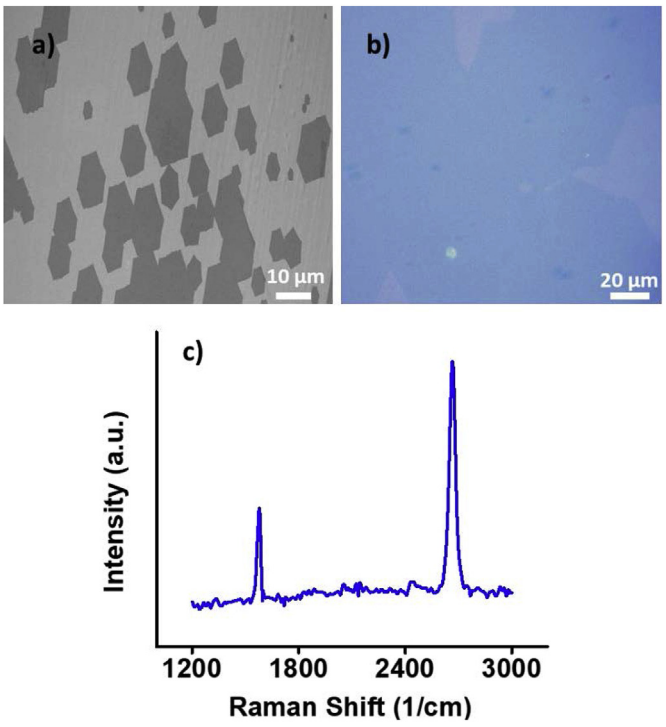

Fig. 1. CVD graphene properties: (a) SEM image of CVD grown graphene on copper substrate (b) Optical image of graphene transferred onto SiO_2 substrate (c) Raman spectra of SL graphene. (A colour version of this figure can be viewed online.)

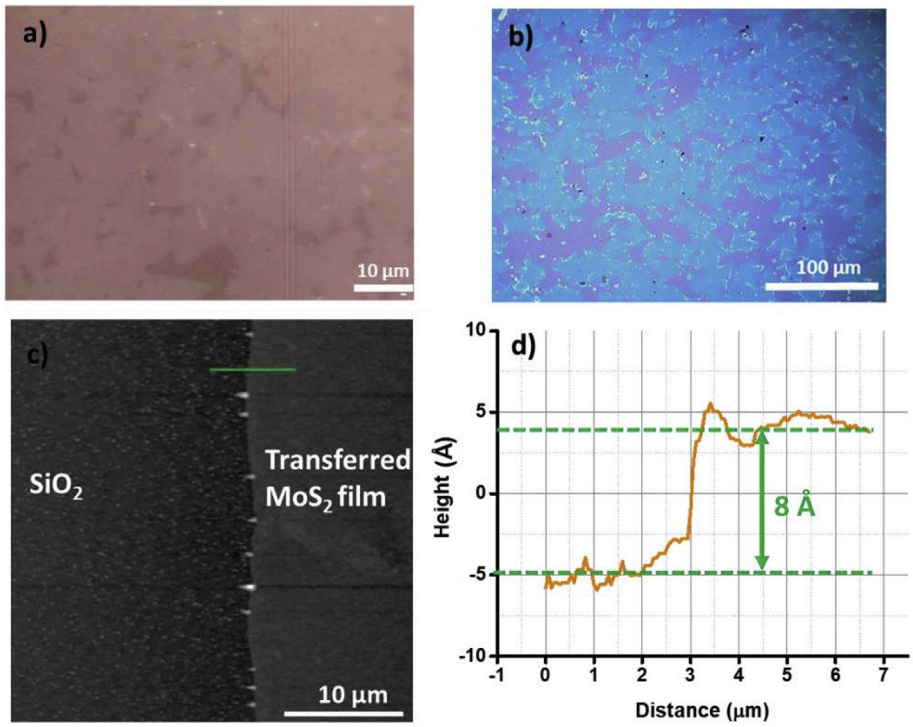

Fig. 2. CVD MoS_2 properties: (a) As-grown CVD MoS_2 on sapphire. (b) As-grown CVD MoS_2 on Si/SiO_2 substrate. (c) AFM Image of MoS_2 film (d) Height profile of MoS_2 film. (A colour version of this figure can be viewed online.)

profile between the two surfaces of SiO_2 substrate and MoS_2 film, shown in Fig. 2(c) and (d), is about 8 Å, which corresponds to SL-MoS_2. [34] Raman spectra of CVD-MoS_2 in Fig. 3(a) illustrates the two significant E_{2g} and A_{1g} peaks, corresponding to the in-plane and out-of-plane vibration modes at 388 cm^{-1} and 407 cm^{-1}, respectively. The distance of ~19–20 cm^{-1} between the two peaks is indicative of monolayer of CVD MoS_2 as reported elsewhere [34]. The band gap of a SL MoS_2 is determined using PL measured under excitation of green laser beam ($\lambda_{ex} = 532$ nm) at low power of 5 mW to avoid local heating. The PL spectra in Fig. 3(b) shows a sharp peak at 675–680 nm of energy, which corresponds to direct band gap of ~1.87 eV. This value agrees with the band gap of SL MoS_2 that has been reported previously [6].

After both individual materials were synthesized, the heterostructure was then fabricated by capping graphene with MoS_2 through a physical transfer method, followed by annealing to promote the contact between two materials. Raman spectra were recorded to ensure the properties of both materials were well-preserved after the transfer process. We also observed insignificant shift in E_{2g} and A_{1g} peaks between the SL MoS_2 and MoS_2/Graphene heterostructure (Fig. S2) which is an indication of contamination free interface [35]. While two E_{2g} and A_{1g} peaks of MoS_2 remain unchanged, a shift in G and 2D peaks of graphene is observed as seen in Fig. 4(a). Unlike a minor shift in the 2D peak, the noticeable redshift, i.e. shift to the right, in G peak confirms the doping of graphene layer due to its interaction with the SL MoS_2 layer, consistent with earlier results [36–38]. On the other hand, PL measurement of MoS_2 in the heterostructure, as seen in Fig. 4(b), finds a significant quench of over 50% in intensity when compared to SL MoS_2. This demonstrates a strong interaction between graphene and MoS_2 layers, and is usually ascribed to charge transfer processes [15,22,35].

For further elucidation of the doping effect due to charge transfer, the electronic properties of back-gated (BG) FETs

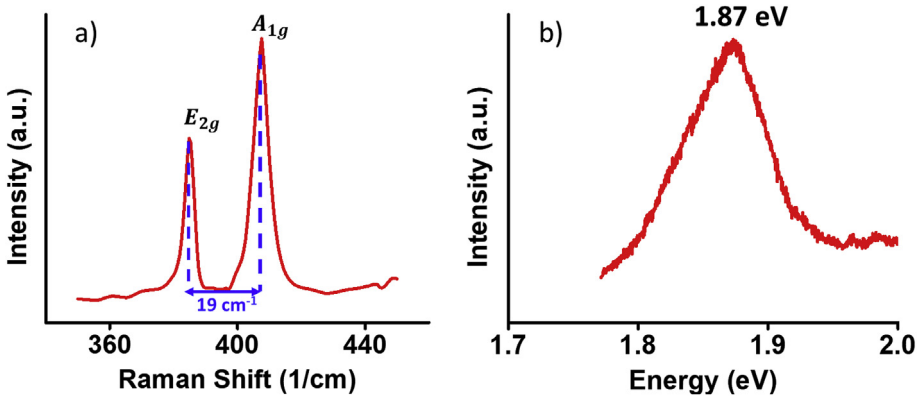

Fig. 3. Raman spectra (a) and PL spectra (b) of SL MoS_2. (A colour version of this figure can be viewed online.)

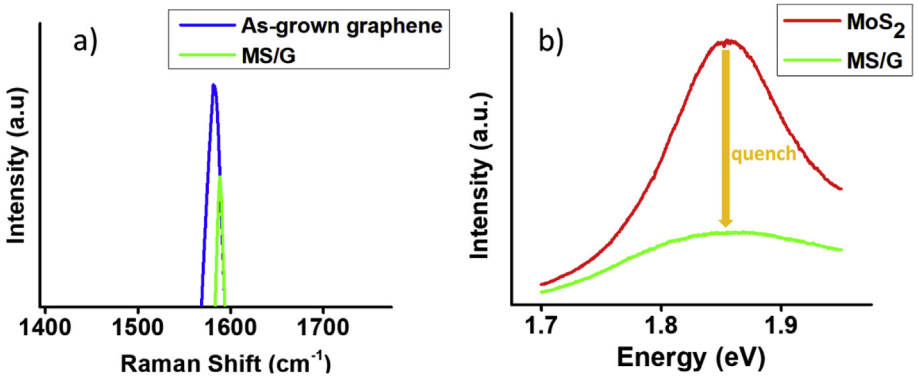

Fig. 4. Raman shift observed at G peak (a) and PL intensity quench (b) in MS/G. (A colour version of this figure can be viewed online.)

fabricated with these materials were investigated. The resulting FET transfer curve was plotted in Fig. 5. The graphene FET shows V_{CNP} at 85 V measured in atmosphere at room temperature, which is typical for a CVD grown graphene [39,40]. This high p-doping of graphene is commonly observed after a photolithography process of patterning involving the use of O_2 plasma and exposure to metal etching solution such as ammonium persulfate (APS) and other adsorbents such as water and oxygen from the atmosphere [41,42]. Even though CVD-graphene is an ambipolar material, the significant difference between the two slopes of the right arm (related to electron concentration) and left arm (related to hole concentration) of the graphene FET's transfer curve indicates holes are the majority carriers in our CVD-graphene based FETs. However, when graphene is fully covered by MoS_2 the V_{CNP} is found at $V_{BG} = 50$ V indicating that graphene capped with MoS_2 becomes less p-doped (i.e more n-doped), due to the transfer of electrons from MoS_2 to graphene. In addition, the electron-to-hole ratio in the heterostructure increases as confirmed by the gain in the slope of the transfer curve's right arm.

In order to understand the fundamentals of doping and charge transport phenomena, the electronic structure and band alignment of the heterostructure is modeled as seen in Fig. 6 and Fig. 7. The MS/G supercell is created by straining the graphene layer. The detail on model design and method used is described in the method section. The site-projected band structure is shown in Fig. 6. Due to the in-built strain and charge transfer, the Fermi-level shifted above the CNP or Dirac point by n-doping the graphene system, as compared to pure SL graphene. In addition, the bi-axial strains also

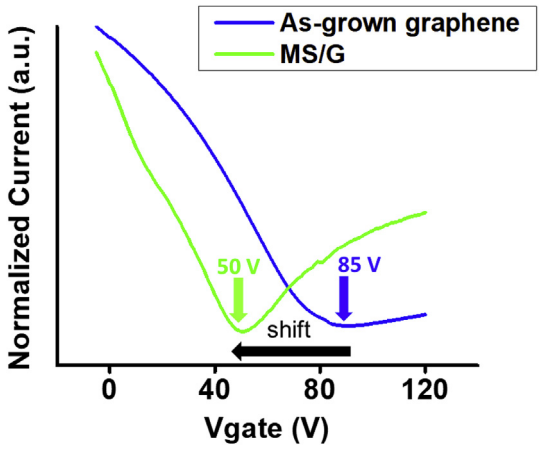

Fig. 5. Transfer curve of as-grown graphene FET and MS/G FET. (A colour version of this figure can be viewed online.)

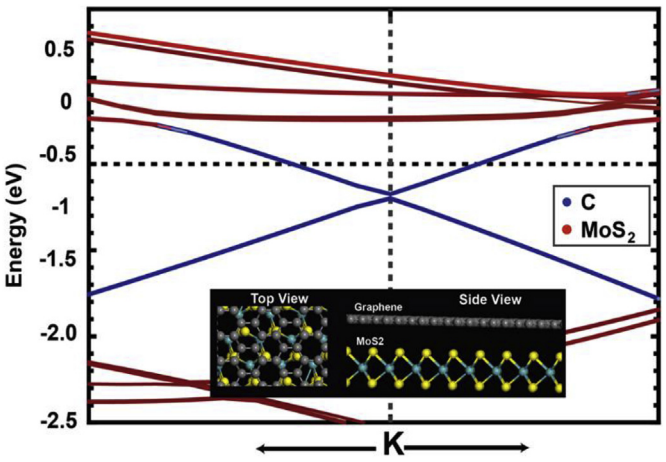

Fig. 6. Band structure of MoS_2/graphene heterostructure. Inset illustrates graphene-MoS_2 model used in our simulation. (A colour version of this figure can be viewed online.)

contribute to the band gap opening in the order of few meV at the Dirac cone of graphene. The origin of the band-gap opening is further confirmed by performing separate band structure calculation for 5% strained graphene layer. The work-functions, which is defined as the energy difference between the Fermi energy and the vacuum levels relative to their vacuum levels, of SL graphene and MS/G heterostructure are illustrated in Fig. 7. Quantitatively, the work-functions of SL graphene and MS/G heterostructure are

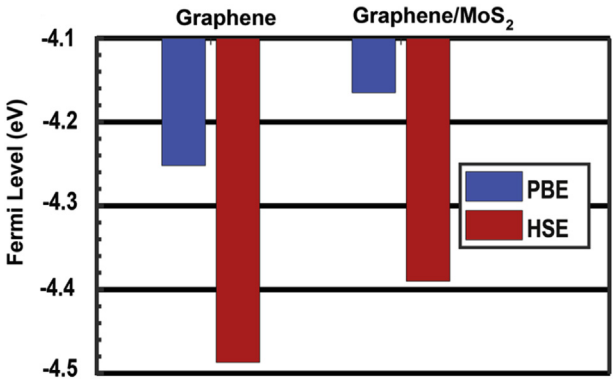

Fig. 7. Comparison of work-function between a SL graphene and MoS_2/graphene heterostructure model used in our simulation. (A colour version of this figure can be viewed online.)

4.487 eV and 4.390 eV, respectively. The work-function difference of 97 meV between the SL graphene and MS/G heterostructure is primarily due to the shift in the Fermi-level resulting from the charge transfer from the MoS_2 layer to graphene layer. This computed value of 97 meV is similar to the change in work function (i.e. shift of Fermi level) measured via UPS method of 100 meV, which is presented in the subsequent section. The small difference may be resulted by variation in work functions of theoretical and as-prepared graphene, namely 4.487 eV and 5.2 eV. The observed in-built Schottky barrier heights (SBH) of the MS/G heterostructure is 127 meV, which is consistent with previous studies [43–45].

To further explore the effect of MoS_2 in the electronic properties of graphene, we obtained the electrochemical impedance of the pristine and heterostructure electrodes with the configuration shown in Fig. 8(a). The impedance is measured at a frequency (f) of 10 kHz while sweeping the potential of the electrode. The electrical double-layer capacitance (C_{EDL}), which can be approximated to the quantum capacitance in graphene, was calculated according to Equation (1), where Z'' is the imaginary part of the complex impedance.

$$C_{EDL} = -\frac{1}{2\pi f Z''} \quad (1)$$

The area-normalized $C_{EDL}$with respect to the electrode potential vs. Ag/AgCl is shown in Fig. 8(b). The C_{EDL} vs. V curves are all concave-shaped with the capacitance suppressed near the CNP, with minimum values between 2 and 3.5 μFcm^{-2}, in agreement to previous reports for four-layer graphene (4LG) [46]. The low C_{EDL} obtained is attributed to the low density of states near or at the Fermi level [47]. The low defect density of our graphene results in C_{EDL} similar to the basal plane of HOPG [48]. The CNP is summarized for each electrode in Fig. 8(c), with a value of −0.02 V for pristine 4LG, close to the values of −0.05 V for 4LG or −0.1 V reported by electrochemical methods for graphene nanoplatelets [34,49]. Mostly no shift is observed for the non-annealed stack of MoS_2/4LG with CNP at −0.03 V, however, after annealing there is a significant shift to −0.18 V. The MoS_2 layer induces a net CNP or Fermi level upshift of 0.16 eV, attributed to doping of the graphene sheet due to electron transfer from MoS_2. Simple physical stacking of MoS_2 as an interlayer does not change the electrochemical behavior of 4LG, annealing is necessary for hybridization of the electronic states of both materials. Annealing removes adsorbed molecules at the interface like O_2 and H_2O, which reduces the interfacial distance between graphene and MoS_2, increasing the electric field that cause charge transfer from one material to the other, i.e. doping [50,51].

The n-doping effect of combining MoS_2 and graphene is explained by band-alignment diagram in Fig. 9. All the parameters used in this diagram are extracted from experiment. CVD-MoS_2 is well-known as an n-type material due to its sulfur vacancies and other lattice impurities [52–54]. On the other hand, CVD-graphene as a highly p-doped material has a Fermi level found closer to the valance band (VB) energy, which results in a higher work-function than that of n-doped MoS_2. In fact, the work-function of graphene measured by UPS is 5.2 eV, which is higher than one of MoS_2 at 4.9 eV. These values are consistent with first principle calculated values for the single layer graphene and MoS_2. As the two materials come in contact forming heterojunction, the difference in their work-function triggers electron transfer from n-type MoS_2 to highly p-doped graphene, and those electrons are then combined with excess holes in graphene. Such mechanism is consistent with the observed reduction in hole concentration from electrochemical measurement of capacitance. As a result, the Fermi level of graphene in the heterostructure shifted up (i.e., less p-doped) resulting in 0.1 eV work-function reduction, as compared to as-grown SL graphene. The CNP shift of +0.1 eV measured with UPS is also close to the value obtained from electrochemical measurements (+0.16 eV) and first principle calculations (+0.097 eV). This is also consistent with the negative shift of V_{CNP} in MS/G FETs in field-effect transfer curve observed in Fig. 5. The reduction in work-function due to the shift in CNP point could be the source of PL intensity quenching observed in MS/G heterostructure, as compared to SL MoS_2. Due to the electron transfer, the number of electrons in MoS_2 reduces, which causes the decrease in the number of electron-hole combination during the PL excitation. Similar n-doping effect is also observed in heterostructure of n-type WS_2 and graphene and expected to further enhance under illumination, which is not discussed in scope of this paper [22,23]. Thus, this finding offers a new method of n-doping graphene for p-

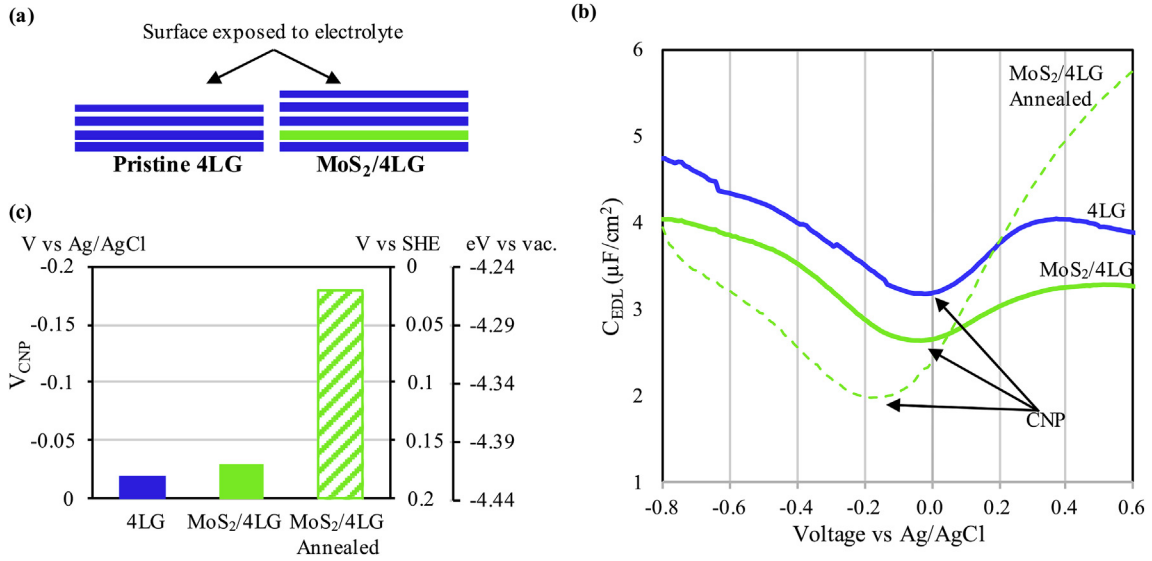

Fig. 8. Electrical double-layer capacitance (C_{EDL}) of 4LG and MoS_2/4LG electrodes. (a) Schematic of 4LG and MoS_2/4LG heterostructure electrodes studied by electrochemical impedance. (b) C_{EDL} plotted vs the electrode potential measured against Ag/AgCl reference electrode calculated form Equation [1]. (c) Potential at charge neutrality point (V_{cnp}) for each electrode. (A colour version of this figure can be viewed online.)

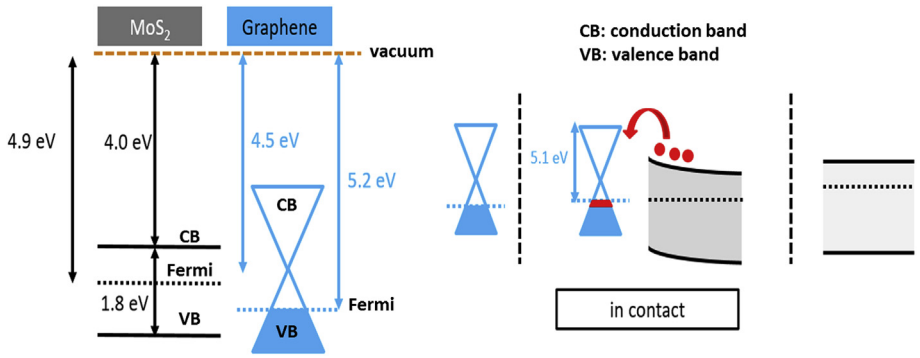

Fig. 9. Band diagram of graphene, MoS_2 and MS/G (in contact). (A colour version of this figure can be viewed online.)

n junction transistor applications without introducing signification defects via conventional doping methods which requires chemical enhancement [55,56].

Utilizing the FET design with MoS_2, graphene and heterostructure as channel materials, we then analyzed the feasibility of these devices as sensors by exposing them to different gaseous analytes. More detail of the gas sensing system is described in the experimental section. Firstly, the stability of the heterostructure device was examined in the presence of dry air. The initial V_{CNP0} was measured before the dry air was introduced to the system (t = 0 min). After the devices stabilized in the continuous air flow for 20 min, the V_{CNP} of the devices were taken every subsequent 5 min. The shift in CNP (ΔCNP) is defined as $\Delta CNP = V_{CNP} - V_{CNP0}$. Therefore, ΔCNP at t = 0 min, by definition, equals 0 V, which is not explicitly plotted in Fig. 10. After the devices stabilize, ΔCNP of graphene FET is measured at 14 V while one of the MS/G FET changes by 3 V. Oxygen, as oxidizing gas molecules, in the dry air contributes to the observed ΔCNP [57]. For the first 20 min, these changes of 3 V vs. 14 V indicates that MS/G is more stable than graphene. In addition, 40 min after the devices stabilize, the MS/G device shows a negligible change of 0.3 V of ΔCNP while ΔCNP of graphene FET increases by an additional 8 V (from 14 V to 22 V). Due to its atomic thickness, SL graphene possesses an exceptionally high surface area-to-volume ratio, deeming its surface highly favorable for gas molecules to adsorb [57]. On the other hand, due to the termination of the existing lone pair of electrons of the sulfur on the surface, MoS_2 behaves more passively and hence its interaction with the ambient environment is negligible. This explains why the MS/G device becomes more stable when graphene is capped with MoS_2. This phenomenon is also seen in other studies where MoS_2 FETs are highly stable for 24 h in wet conditions and at different pH conditions [58]. As a result, MoS_2 in such a heterostructure acts as a protective layer on graphene to minimize the atmospheric interference, which can lead to inaccuracies in gas sensing.

Taking advantage of the stability of the heterostructure, we investigated the sensing properties using CNP shift as an alternative to the traditional transient response. FET devices using MS/G as a conducting channel were exposed to different concentrations of NO_2 in dry air. The result is shown in Fig. 11. In this experiment, ΔCNP is defined the same as above. V_{CNP0} was first taken after 20 min of device stabilization in dry air. Each concentration of NO_2 was introduced to the gas chamber for 20 min to achieve saturation, and measurement of V_{CNP} was then recorded. From the previous FET transfer characteristics curves, MS/G FETs shows p-type behavior at $V_{BG} = 0$ V. Upon binding to typical electron-withdrawing gas molecules (NO_2), electrons are withdrawn from the conducting material and hence causes the increase in hole concentration of the materials, which in turn enhances the p-type doping effect. As a result, the CNP of the device then shifts to the positive direction of V_{BG}. As the concentration of NO_2 increases, more holes accumulates in the material and subsequently greater p-doping effect is observed as represented by the upshifting of CNP. It is also noticed in Fig. 10 that the shift of CNP in MS/G during the exposure to NO_2 at our lowest tested concentration of 200 ppm, is 8 times higher than in the control experiment in presence of pure dry

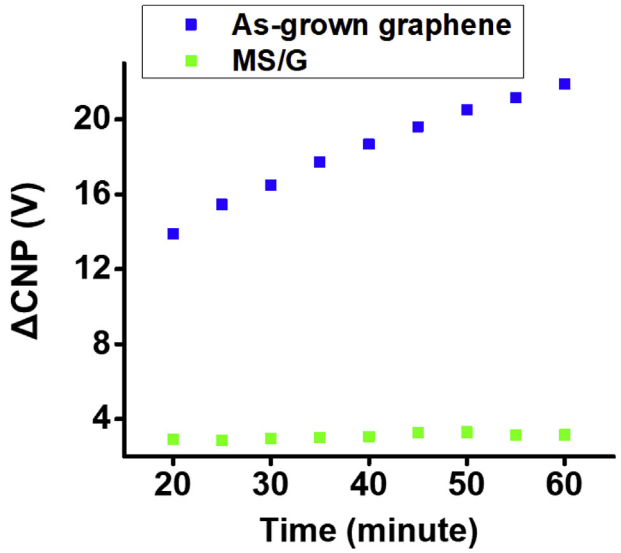

Fig. 10. ΔCNP of graphene and MS/G FET devices in dry air. (A colour version of this figure can be viewed online.)

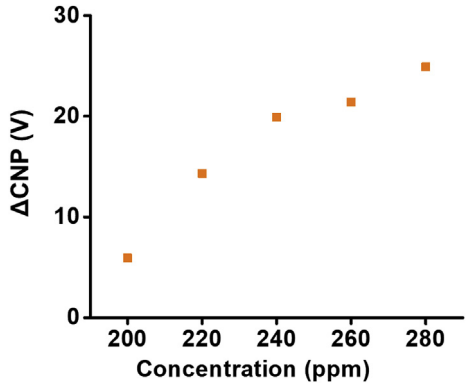

Fig. 11. ΔCNP of MS/G FET devices in presence of NO_2. (A colour version of this figure can be viewed online.)

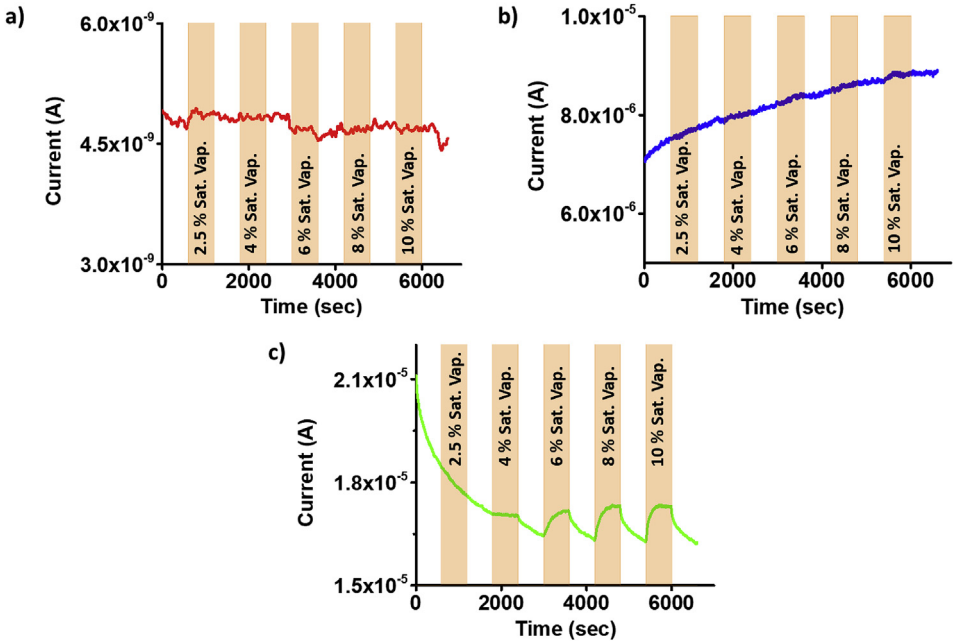

Fig. 12. Dynamic response of (a) MoS_2, (b) graphene and (c) MS/G FET devices in presence of toluene at $V_{source\text{-}drain} = 0.1$ V and $V_{bg} = 0$.

air. This ensures the shift of CNP is due to the interaction between the analyte gas NO_2 and the sensing materials.

We also investigated the dynamic response of the MS/G heterostructure-based devices with volatile organic compounds. Toluene is chosen as a candidate analyte for our experiment because it has been widely used as a solvent for paint, glue, rubber or varnish industries, etc. However, exposure to high concentration of toluene at thousands of ppm may cause extreme damage to human health [59]. In addition, its higher binding affinity to MoS_2 than to graphene makes toluene a perfect candidate for comparison between MS/G, MoS_2 and graphene [39,41,60]. Fig. 12 shows sensing responses, current output, of FET devices with the three materials as sensing channel at varying concentrations of toluene vapors. As expected, due to a low binding affinity of toluene to graphene, the graphene-based FET device shows no response at investigated concentrations (Fig. 12(b)). However, the MoS_2-based FET device, despite having a higher binding affinity to toluene, still experiences an extremely low signal-to-noise ratio due to a high contact resistance and low electrical mobility (Fig. 12(a)). On the other hand, the MS/G sensing channel device exhibited a high response, approximately 12.5% change in current within 10 min at the concentration of 10% of saturated vapor at room temperature (Fig. 12(c)). The response is ascribed to an increase in concentrations of holes in the p-type MS/G FET device (at $V_{BG} = 0$ V) upon binding of electron-withdrawing toluene gas molecules to the sensing channel. This suggests a superior application of the MS/G material over the constituent materials due to the increased stability, sensitivity and signal-to-noise ratio.

4. Conclusion

In this study, the n-doping effect was investigated in a vertically stacked heterostructure of MoS_2 and graphene. The FET characteristics transfer curve confirms the highly p-doped graphene attributed to both the CVD process of synthesis and the device fabrication process. This graphene becomes less p-doped in its heterostructure as observed by a shift of CNP from a high back-gate voltage of 85 V to a smaller value of 50 V. The electron transfer from MoS_2 to graphene in the annealed heterostructure is further confirmed by the shift of the graphene Raman peaks, the PL quenching of the MoS_2, a shift of CNP in C_{EDL} vs V curve measured in electrochemical setup, and the reduction in work-function measured by UPS and predicted by first principle simulations. In addition, the top MoS_2 layer in the heterostructure performs as a passive layer on graphene, which successfully minimizes the electrical drifting due to the strong interaction between the sensing channel and the ambient atmosphere. Hence, this new method of gas sensing using a shift of CNP is novel and efficient, as compared to traditional amperometric measurement. Finally, the study of the MoS_2/graphene heterostructure as a channel material for sensing applications to the volatile gas molecules, such as toluene, suggests it as a novel material with high sensitivity and stability for gas detection.

Acknowledgments

This research was funded by grants from the National Science Foundation (1842718) and UC Riverside and Korea Institute of Materials Science (Research Program (POC2930)) through UC-KIMS Center for Innovation Materials for Energy and Environment.

Appendix A. Supplementary data

Supplementary data to this article can be found online at https://doi.org/10.1016/j.carbon.2018.10.079.

References

[1] P. Ajayan, P. Kim, K. Banerjee, Two-dimensional van der Waals materials, Phys. Today 69 (2016) 38–44.
[2] K.S. Novoselov, A.K. Geim, S.V. Morozov, D. Jiang, Y. Zhang, S.V. Dubonos, I.V. Grigorieva, A.A. Firsov, Electric field effect in atomically thin carbon films, Science 306 (2004) 666–668.
[3] I. Meric, M.Y. Han, A.F. Young, B. Ozyilmaz, P. Kim, K.L. Shepard, Current saturation in zero-bandgap, top-gated graphene field-effect transistors, Nat. Nanotechnol. 3 (2008) 654–659.
[4] M. Xu, T. Liang, M. Shi, H. Chen, Graphene-like two-dimensional materials, Chem. Rev. 113 (2013) 3766–3798.
[5] C. Lee, H. Yan, L.E. Brus, T.F. Heinz, J. Hone, S. Ryu, Anomalous lattice vibrations of single- and few-layer MoS_2, ACS Nano 4 (2010) 2695–2700.

[6] K.F. Mak, C. Lee, J. Hone, J. Shan, T.F. Heinz, Atomically thin MoS_2: a new direct-gap semiconductor, Phys. Rev. Lett. 105 (2010), 136805.
[7] B. Radisavljevic, A. Radenovic, J. Brivio, V. Giacometti, A. Kis, Single-layer MoS_2 transistors, Nat. Nanotechnol. 6 (2011) 147–150.
[8] K.S. Novoselov, D. Jiang, F. Schedin, T.J. Booth, V.V. Khotkevich, S.V. Morozov, A.K. Geim, Two-dimensional atomic crystals, Proc. Natl. Acad. Sci. U. S. A 102 (2005) 10451–10453.
[9] N. Kaushik, A. Nipane, F. Basheer, S. Dubey, S. Grover, M.M. Deshmukh, S. Lodha, Schottky barrier heights for Au and Pd contacts to MoS_2, Appl. Phys. Lett. 105 (2014), 113505.
[10] Y.J. Yu, Y. Zhao, R. Ryu, L.E. Brus, K.S. Kim, P. Kim, Tuning the graphene work function by electric field effect, Nano Lett. 9 (2009) 3430–3434.
[11] C.H. Lee, G.H. Lee, A.M. van der Zande, W. Chen, Y. Li, M. Han, X. Cui, G. Arefe, C. Nuckolls, T.F. Heinz, J. Guo, J. Hone, P. Kim, Atomically thin P–n junctions with van der Waals heterointerfaces, Nat. Nanotechnol. 9 (2014) 676–681.
[12] S. Rathi, I. Lee, D. Lim, J. Wang, Y. Ochiai, N. Aoki, K. Watanabe, T. Taniguchi, G.H. Lee, Y.J. Yu, P. Kim, G.H. Kim, Tunable electrical and optical characteristics in monolayer graphene and few-layer MoS_2 heterostructure devices, Nano Lett. 15 (2015) 5017–5024.
[13] Y.C. Lin, R.K. Gosh, R. Addou, N. Lu, S.M. Eichfeld, H. Zhu, M.Y. Li, X. Peng, M.J. Kim, L.J. Li, R.M. Wallace, S. Datta, J.A. Robinson, Atomically thin resonant tunnel diodes built from synthetic van der Waals heterostructures, Nat. Commun. 6 (2015) 7311.
[14] Y.C. Lin, N. Lu, N.P. Lopez, J. Li, Z. Lin, X. Peng, C.H. Lee, C. Sun, L. Calderin, P.N. Browning, M.S. Bresnehan, M.J. Kim, T.S. Mayer, M. Terrones, J.A. Robinson, Direct synthesis of van der Waals solids, ACS Nano 8 (2014) 3715–3723.
[15] Y. Shi, W. Zhou, A.Y. Lu, W. Fang, Y.H. Lee, A.L. Hsu, S.M. Kim, K.K. Kim, H.Y. Yang, L.J. Li, J.C. Idrobo, J. Kong, Van der Waals epitaxy of MoS_2 layers using graphene as growth templates, Nano Lett. 12 (2012) 2784–2791.
[16] W. Yang, G. Chen, Z. Shi, C.C. Liu, L. Zhang, G. Xie, M. Cheng, D. Wang, R. Yang, D. Shi, K. Watanabe, T. Taniguchi, Y. Yao, Y. Zhang, G. Zhang, Epitaxial growth of single-domain graphene on hexagonal boron nitride, Nat. Mater. 12 (2013) 792–797.
[17] Y. Gong, J. Lin, X. Wang, G. Shi, S. Lei, Z. Lin, X. Zou, G. Ye, R. Vajtai, B.I. Yakobson, H. Terrones, M. Terrones, B.K. Tay, J. Lou, S.T. Pantelides, Z. Liu, W. Zhou, P.M. Ajayan, Vertical and in-plane heterostructures from WS_2/MoS_2 monolayers, Nat. Mater. 13 (2014) 1135–1142.
[18] M.P. Levendorf, C.J. Kim, L. Brown, P.Y. Huang, R.W. Havener, D.A. Muller, J. Park, Graphene and boron nitride lateral heterostructures for atomically thin circuitry, Nature 488 (2012) 627–632.
[19] F.K. Perkins, A.L. Friedman, E. Cobas, P.M. Campbell, G.G. Jernigan, B.T. Jonker, Chemical vapor sensing with monolayer MoS_2, Nano Lett. 13 (2013) 668–673.
[20] F. Schedin, A.K. Geim, S.V. Morozov, E.W. Hill, P. Blake, M.I. Katsnelson, K.S. Novoselov, Detection of individual gas molecules adsorbed on graphene, Nat. Mater. 6 (2007) 652–655.
[21] J. Kong, N.R. Franklin, C. Zhou, M.G. Chapline, S. Peng, K. Cho, H. Dai, Nanotube molecular wires as chemical sensors, Science 287 (2000) 622–655.
[22] H. Tan, Y. Fan, Y. Rong, B. Porter, C.S. Lau, Y. Zhou, Z. He, S. Wang, H. Bhaskaran, J.H. Warner, Doping graphene transistors using vertical stacked monolayer WS_2 heterostructures grown by chemical vapor deposition, ACS Appl. Mater. Interfaces 8 (2016) 1644–1652.
[23] N. Huo, Z. Wei, X. Meng, J. Kang, F. Wu, S.S. Li, S.H. Wei, J. Li, Interlayer coupling and optoelectronic properties of ultrathin two-dimensional heterostructures based on graphene, MoS_2 and WS_2, J. Mater. Chem. C 3 (2015) 5467–5473.
[24] D. De Fazio, I. Goykhman, D. Yoon, M. Bruna, A. Eiden, S. Milana, U. Sassi, M. Barbone, D. Dumcenco, K. Marinov, A. Kis, A.C. Ferrari, High responsivity, large-area graphene/MoS_2 flexible photodetectors, ACS Nano 10 (2016) 8252–8262.
[25] H. Malekpour, P. Ramnani, S. Srinivasan, G. Balasubramanian, D.L. Nika, A. Mulchandani, K. Roger, R.K. Lake, A.A. Balandin, Thermal conductivity of graphene with defects induced by electron beam irridiation, Nanoscale 8 (2016) 14608–14616.
[26] J.P. Perdew, K. Burke, M. Ernzerhof, Generalized gradient approximation made simple, Phys. Rev. Lett. 77 (1996) 3865–3868.
[27] M. Ernzerhof, G. Scuseria, Assessment of the perdew-burke-ernzerhof exchange-correlation functional, J. Chem. Phys. 110 (1999) 5029.
[28] G. Kresse, J. Hafner, Ab initio molecular dynamics for liquid metals, Phys. Rev. B 47 (1993) 558.
[29] J. Heyd, G.E. Scuseria, M. Ernzerhof, Hybrid functionals based on a screened coulomb potential, J. Chem. Phys. 118 (2003) 8207.
[30] S. Grimme, Semiempirical GGA-type density functional constructed with a long-range dispersion correction, J. Comput. Chem. 27 (2006) 1787–1799.
[31] P. Lazic, CellMatch: combining two unit cells into a common supercell with minimal strain, Comput. Phys. Commun. 197 (2015) 324–334.
[32] R. Beams, L.G. Cançado, L. Novotny, Raman characterization of defects and dopants in graphene, J. Phys. Condens. Matter 27 (2015), 083002.
[33] Z. Ni, Y. Wang, T. Yu, Z. Shen, Raman spectroscopy and imaging of graphene, Nano Res 1 (2008) 273–291.
[34] Y. Zhan, Z. Liu, S. Najmaei, P.M. Ajayan, J. Lou, Large-area vapor-phase growth and characterization of MoS_2 atomic layers on A SiO_2 substrate, Small 8 (2012) 966–971.
[35] L. Liang, J. Zhang, B.G. Sumpter, Q.H. Tan, P.H. Tan, V. Meunier, Low-frequency shear and layer-breathing modes in Raman scattering of two-dimensional materials, ACS Nano 11 (2017) 11777–11802.
[36] Li, Y. Intrinsic doping dependence of Raman 2D mode in graphene: signatures of electron-electron interaction. In: Probing the Response of Two-dimensional Crystals by Optical Spectroscopy (pp. 9-18). Springer Theses (Recognizing Outstanding Ph.D. Research). Springer, Cham.
[37] C. Stampfer, L. Wirtz, A. Jungen, D. Graf, F. Molitor, C. Hierold, K. Ensslin, Raman imaging of doping domains in graphene on SiO_2, Appl. Phys. Lett. 91 (2007), 241907.
[38] T. Pandey, A.P. Nayak, S.T. Moran, J.S. Kim, L.J. Li, J.F. Lin, D. Akinwande, A.K. Singh, Pressure-induced charge transfer doping of monolayer graphene/MoS_2 heterostructure, Small 12 (2016) 4063–4069.
[39] S. Peng, Z. Jin, P. Ma, G.H. Yu, J.Y. Shi, D.Y. Zhang, J. Chen, X.Y. Liu, T.C. Ye, Heavily P-type doped chemical vapor deposition graphene field-effect transistor with current saturation, Appl. Phys. Lett. 103 (2013), 223505.
[40] S. Goniszewski, M. Adabi, O. Shaforost, S.M. Hanham, L. Hao, N. Klein, Correlation of P-doping in CVD graphene with substrate surface charges, Sci. Rep. 6 (2016) 22858.
[41] K. Kim, H.H.J. Park, B.C. Woo, K.J. Kim, G.T. Ki, W.S. Yun, Electric property evolution of structurally defected multilayer graphene, Nano Lett. 8 (2008) 3092–3096.
[42] B.B. Kantar, M. öZtüRk, H. çEtin, The effects of lithographic residues and humidity on graphene field effect devices, Bull. Mater. Sci. 40 (2017) 239–245.
[43] L. Yu, Y.H. Lee, X. Ling, E.J.G. Santos, Y.C. Shin, Y. Lin, M. Dubey, E. Kaxiras, J. Kong, H. Wang, T. Palacios, Graphene/MoS_2 hybrid technology for large-scale two-dimensional electronics, Nano Lett. 14 (2014) 3055–3063.
[44] J. Yoon, W. Park, G.Y. Bae, Y. Kim, H.S. Jang, Y. Hyun, S.K. Lim, Y.H. Kahng, W.K. Hong, B.H. Lee, H.C. Ko, Highly flexible and transparent multilayer MoS_2 transistors with graphene electrodes, Small 9 (2013) 3295–3300.
[45] W.J. Yu, Z. Li, H. Zhou, Y. Chen, Y. Wang, Y. Huang, X. Duan, Vertically stacked multi-heterostructures of layered materials for logic transistors and complementary inverters, Nat. Mater. 12 (2013) 246–252.
[46] H. Ji, X. Zhao, Z. Qiao, J. Jung, J. Zhu, Y. Lu, L.L. Zhang, A.H. MacDonald, R.S. Ruoff, Capacitance of carbon-based electrical double-layer capacitors, Nat. Commun. 5 (2014) 3317.
[47] M.A. Pope, I.A. Aksay, Four-fold increase in the instrinsic capacitance of graphene through functionalization and lattic disorder, J. Phys. Chem. C 119 (2015) 20369–20378.
[48] H. Gerischer, R. McIntyre, D. Scherson, W. Storck, Density of the electronic states of graphite: derivation from differential capacitance measurements, J. Phys. Chem. 91 (1987) 1930–1935.
[49] J.H. Kim, J. Lee, C.C. Hwang, C. Lee, J.Y. Park, Work function variation of MoS_2 atomic layers grown with chemical vapor deposition: the effects of thickness and the adsorption of water/oxygen molecules, Appl. Phys. Lett. 106 (2015), 251606.
[50] L. Janicki, G. Kunert, M. Sawicki, E. Piskorska-Hommel, K. Gas, R. Jakiela, D. Hommel, R. Kudrawiec, Fermi level and bands offsets determination in insulating (Ga,Mn)N/GaN structures, Sci. Rep. 7 (2017) 41877.
[51] J. Poon, C. Batchelor-McAuley, K. Tschulik, R.G. Compton, Single graphene nanoplatelets: capacitance, potential of zero charge and diffusion coefficient, Chem. Sci. 6 (2015) 2869–2876.
[52] X. Tong, E. Ashalley, F. Lin, H. Li, Z.M. Wang, Advances in MoS_2-based field effect transistors (FETs), Nano-Micro Lett. 7 (2015) 203–218.
[53] J. Kang, W. Liu, K. Banerjee, High-performance MoS_2 transistors with low-resistance molybdenum contacts, Appl. Phys. Lett. 104 (2014), 093106.
[54] S.D. Namgung, S. Yang, K. Park, A.J. Cho, H. Kim, J.Y. Kwon, Influence of post-annealing on the off current of MoS_2 field-effect transistors, Nanoscale Res. Lett. 10 (2015) 1.
[55] K. Brenner, R. Murali, Single step, complementary doping of graphene, Appl. Phys. Lett. 96 (2010), 063104.
[56] D. Xiang, C. Han, J. Wu, S. Zhong, Y. Liu, J. Lin, X.A. Zhang, W.P. Hu, B. Ozyilmaz, A.H. Castro Neto, A.T.S. Wee, W. Chen, Surface transfer doping induced effective modulation on ambipolar characteristics of few-layer black phosphorus, Nat. Commun. 6 (2015) 6485.
[57] L. Kong, A. Enders, T.S. Rahman, P.A. Dowben, Molecular adsorption on graphene, J. Phys. Condens. Matter 26 (2014) 443001.
[58] D.W. Lee, J. Lee, I.Y. Sohn, B.Y. Kim, Y.M. Son, H. Bark, J. Jung, M. Choi, T.H. Kim, C. Lee, N.E. Lee, Field-effect transistor with a chemically synthesized MoS_2 sensing channel for label-free and highly sensitive electrical detection of DNA hybridization, Nano Res 8 (2015) 2340–2350.
[59] L.K. Low, J.R. Meeks, C.R. Mackerer, Health effects of the alkylbenzenes. I. Toluene, Toxicol. Ind. Health 4 (1988) 49–75.
[60] R. Samnakay, C. Jiang, S.L. Rumyantsev, M.S. Shur, A.A. Balandin, Selective chemical vapor sensing with few-layer MoS_2 thin-film transistors: comparison with graphene devices, Appl. Phys. Lett. 106 (2015), 023115.